Compressive properties and micro-structural characteristics of Ti-6Al-4V fabricated by electron beam melting and selective laser melting

Lijun Xiao[a], Weidong Song[a1], Menglei Hu[a], Peifeng Li[b]

[a] State Key Laboratory of Explosion Science and Technology, Beijing Institute of Technology, Beijing 100081, China
[b] School of Engineering, University of Glasgow, Glasgow, UK

ABSTRACT

Bulk Ti-6Al-4V material and its lattice structures with rhombic dodecahedron unit cells are fabricated by electron beam melting (EBM) and selective laser melting (SLM) method respectively. The effect of part size on the compressive properties and failure modes of the material is taken into consideration. Electronic universal testing machine and Split Hopkinson pressure bar (SHPB) system are adopted for experiments, and the compressive behavior of the additively manufactured materials is investigated accordingly. Meanwhile, multiscale observations are conducted to reveal the macro- and microscopic deformation mechanism. The results showed that the mechanical response of the dense struts as well as micro-lattice structures manufactured by the two processes are quite different. The yield strength of the EBM printed parts, in which the grain size distributions and texture between the center and the edge regions seem to be different, are more sensitive to the specimen size. The geometric imperfections are also considered to reduce the strength of the undersized struts prepared by EBM. The specimens fabricated by both of the two approaches exhibit elastic-plastic deformation. Besides, the SLM made material is found to be more sensitive to strain rate especially for that below 1000/s than the EBM parts.

Keywords: Ti-6Al-4V; electron beam melting; selective laser melting; mechanical behavior; microstructure

1 Introduction

Titanium alloys have been widely used as structural components in the aerospace, automotive and shipbuilding industries due to their combination of many excellent properties such as low weight, superior mechanical performance and prominent thermal/corrosion resistance [1]. Ti-6Al-4V alloy, which is a type of 'α+β' dual-phase material, has been the most popular titanium alloy for industrial application. In Ti-6Al-4V alloy, the softer α-phase provides Ti-6Al-4V workability while the harder β phase provides its high strength [2]. Besides, the α/β interface is also reported to influence the fracture behavior of the material [3]. Currently, the rapid development of additive manufacturing (AM) provides a new approach to fabricate Ti-6Al-4V alloy and the corresponding structural equipment, but numerous investigation on the properties of materials need to be conducted before they can be applied extensively.

Selective laser melting is a kind of AM method which uses laser as the heat source. Four main parameters during the fabrication process are the laser power, scan speed, hatch speed and layer thickness [4]. Detailed description of SLM processes has been presented by Kruth et.al [5]. Some literature about the research on SLM manufactured Ti-6Al-4V has been reported. It has been presented that the SLM-printed Ti-6Al-4V consists of a fine acicular martensite phase (α' phase), which relates to a high yield strength (almost 1GPa) and ultimate tensile strength with low ductility (less than 10%) [6,7]. Facchini et.al [8] indicated that the low ductility of SLM Ti-6Al-4V components was caused by the residual stress and the martensitic microstructure. Attar [9] and Chlebus [10] attributed the anisotropic behavior of the SLM parts to the defects inside the materials.

[1] Corresponding author. Tel: +86-10-68914152
E-mail address: swdgh@bit.edu.cn

Simonelli et.al [11] investigated the effect of build orientation on the tensile properties of Ti-6Al-4V, and discussed the mechanical anisotropy and fracture mechanisms in relation to the crystallographic texture. Khorasani et.al [12] conducted detailed research to detect the influence of SLM processing parameters including the laser power, scan speed, hatch space, laser pattern angle coupling and post-heat-treatment on the hardness, density, mechanical performance and surface quality of the printed parts. Vrancken et.al [13] examined the effect of heat treatment on the mechanical behavior and microstructure of SLM processed Ti-6Al-4V, in which the influence of temperature, time and cooling rate were discussed. Qiu et.al [14] tested the Ti-6Al-4V samples with stress relief treatment and hot isostatically pressed (HIPed), and found that the HIP treatment could help to improve the ductility but the strength was reduced. Yang et.al [15] explored the formation and evolution mechanisms of martensites in SLM Ti-6Al-4V, and investigated the effect of processing parameters such as hatch spacing and scanning velocity on the martensitic size, which demonstrated that the martensitic size could be controlled by adjusting the SLM processing parameters.

Electron beam melting (EBM) is another kind of AM method using electron beam as the heat source. When the high speed electron beam interacts with the powder layer, kinetic energy is converted into thermal energy and results in the melting of the powder [4]. Compared with SLM, the penetration depth into the irradiated material by the electron beam is much greater [16]. Main parameters during EBM process include inter-build variations (such as chemistry and build plate temperature) and intra-build variations (such as energy input, location, part size and build orientation) [17, 18]. Hrabe et.al [17] indicated that the distance from the build plate had no influence on the processed parts, but the part size might affect the yield strength (YS) and ultimate tensile strength (UTS) slightly. Besides, they also found that higher energy input led to lower YS, UTS and microhardness, while the build orientation only influenced the elongation [18]. Al-Bermani et.al [19] found that the microstructure and mechanical properties of EBM Ti-6Al-4V exhibited significant dependent on the build temperature. Tan et.al [20] observed that the β phase formed as discrete flat rods were embedded in continuous α phase, and the material exhibited graded microstructure as the β grain width and β phase interspacing increased continuously with the build height. Due to the graded microstructure, the mechanical properties of EBM printed Ti-6Al-4V were found to be graded. Murr et.al [21] compared the EBM fabricated Ti-6Al-4V with wrought Ti-6Al-4V, concluded the graded properties of EBM products and better ductility than the wrought samples. Lu et.al [22] systematically analyzed the microstructure transformation of Ti-6Al-4V during EBM process, which provided helpful strategy for Ti-6Al-4V microstructural optimization. Some other researchers investigated the effect of surface quality and post-treatment on the mechanical properties of EBM printed parts. Formanoir et.al [23] paid attention to the effect of surface finish on the tensile properties of EBM produced Ti-6Al-4V, and found that the surface defects might decrease the yield strength which could be modified by mechanical polishing (removal of the surface defects). Additionally, they also proposed that the chemical etching treatment could increase the relative stiffness of electron beam melted Ti-6Al-4V octet-truss lattice structures as the surface roughness of the strut was significantly decreased [24]. Lhuissier et.al [25] conducted detailed research on the evolution of the strut morphology and the elastic mechanical properties of the specimens with the etching time, which provided an effective method to minimize the surface defects and promote the mechanical behavior of EBM produced complex stuctures.

Although the microstructures and mechanical properties of Ti-6Al-4V components respectively manufactured by SLM and EBM have been compared [4, 6], limited research has been conducted to compare the differences with the part size varies. Additionally, testing system with high precision is needed to investigate the compressive properties of specimens at a micrometer scale. Metallic micro-lattice structures, which comprise an assembly of micro-struts, can be adopted to evaluate the basic properties of the material with tiny sizes due to their properties are related to a single strut. Up to today, a number of studies have also been performed to discuss the properties of additively manufactured Ti-6Al-4V lattice structures[26-35]. Mines [26] fabricated cellular Ti-6Al-4V and stainless steel with Body-Center-Cubic (BCC) structure by adopting SLM technology, found that the surface quality of Ti-6Al-4V strut was much worse than that of stainless steel strut. Leva [27] investigated the influence of energy input on the porosity, constituent, microstructure and mechanical properties of porous titanium parts obtained by SLM. They found that higher energy input could lead to parts with better mechanical properties. Tancogne-Dejean et.al [28] researched the dynamic performance of SLM manufactured metallic micro-lattice structure, analyzing the strut

orientation dependency of material texture.. Xiao et.al [33, 34] tested the compressive behavior of EBM processed Ti-6Al-4V lattice structures under different loading velocities, revealed that the manufactured material can be applied as energy absorber at elevated temperature. They also measured the dynamic response of graded Ti-6Al-4V lattice structures fabricated by SLM method [35]. However, the comparison between the micro-lattice structures fabricated by these two method has been scarcely reported.

This study aims to investigate the compressive behavior and microstructural characteristics of Ti-6Al-4V with various dimensions manufactured by EBM and SLM processes, respectively. Dense Ti-6Al-4V cylinders with four different sizes and open-cell rhombic dodecahedron Ti-6Al-4V lattice structures are fabricated for experimentally research. Quasi-static and dynamic tests are conducted to obtain the compressive stress-strain relationships and failure modes of the struts and lattice structures. Metallographic observations and EBSD analysis are conducted to reveal the microstructure and texture of the specimens. Afterwards, the effect of fabrication processes as well as specimen size on the macroscopic behavior of the additively-manufactured materials is discussed.

2 Experimental procedures

2.1 Material fabrication

Ti-6Al-4V alloy and the corresponding micro-lattice materials in the present study are manufactured through EBM and SLM processes. The EBM process is performed on an ARCAM A2 system which has been introduced elsewhere [36, 37]. The particle diameter of gas-atomized extra low interstitial (ELI) grade Acram Ti-6Al-4V powder adopted for fabrication varies from 30μm to 120μm with an average data of 100μm. The powder-bed is with a depth of 50μm and the layer thickness adopted here is 70μm. Before being melted, the powder is preheated to 720~730℃ layer by layer with a scanning velocity ranging from 0.2 to 10m/s. The electron beam is accelerated with a voltage of 60kV while the beam current is not greater than 35mA. During the melting process, the beam current is reduced to 18mA and the scanning speed is about 0.5m/s. The SLM process is conducted on a BLT-S300 system provided by Xi'an Bright Laser Technologies LTD. The Ti-6Al-4V powder is supplied by EOS with an average diameter of about 100μm. The power of laser used for melting is 400W and the beam diameter is 100μm. The layer thickness adopted for fabrication is 50μm and the scanning speed is approximate 1.5m/s. As the powder is not preheated in SLM process, heat treatment has to be conducted after the manufacture process. Duplex anneal is the most common treatment to achieve stable microstructure and properties of titanium alloys. Firstly, the as-built materials are heated to 650℃(±10℃) in a vacuum environment and kept for 2~4 hours which are cooled in the furnace filled with Argon gas. In this step, the microstructure of the material keeps unchanged and the residual stress in the built parts can be primarily relieved. Afterwards, the materials are heated to 800℃(±10℃) again in a vacuum environment for 2 hours and followed by the same cooling steps as above. During this process, the residual stress in the materials can be totally eliminated and the metastable β phase is completely decomposed to obtain the homogeneous microstructure and property. The above heat treatment parameters are optimized by the specimen supplier (Xi'an Bright Laser Technologies LTD).

2.2 Macro- and microscopic characterization

In order to determine the properties of additively-manufactured fully dense Ti-6Al-4V alloy, four groups of cylindrical Ti-6Al-4V struts with four different diameters (Φ2mm, Φ4mm, Φ6mm, Φ8mm) and a uniform length of 80mm are manufactured by the two additive manufacture methods initially. The strut dimensions are measured after manufacturing using a 0.02 mm precision Vernier caliper. The deviations between the designed diameter and the measured value are presented in Table.1, which verifies that the EBM and SLM processes can guarantee excellent repeatability and high precision.

Table.1 Comparison between the designed diameter and measured data

Designed diameter(mm)	Diameter obtained by EBM (mm)	Deviation (%)	Diameter obtained by SLM (mm)	Deviation (%)

8	8.04	0.5	8.02	0.25
6	5.96	-0.6	6.03	0.5
4	4.04	1	4.02	0.5
2	2.04	2	2.03	1.5

Metallographic specimens are sectioned from the cylindrical Ti-6Al-4V parts along both their building axis and in-plane direction which are displayed in Fig.1. Before being etched by Kroll's reagent (2% HF + 6% HNO_3 + 92% H_2O), the specimens are mechanically ground and polished. Afterwards, optical microscopy (OM) and scanning electron microscopy (SEM) are adopted for microstructural characterization. OM is conducted on an Olympus optical microscope while SEM is carried out on a scanning electron microscope Hitachi S4800. SEM-EDS (energy dispersive spectroscopy) is used to compare the compositional differences in characteristic zones. In order to reveal the crystal characteristics such as the crystal size and texture of the materials, electron backscattered diffraction (EBSD) analysis is performed with an integrated Oxford/NordlysNano EBSD detector. A step size of 0.2μm is chosen to optimize the resolution without increasing too much acquisition time, and the EBSD data are analyzed by Channel 5 software. Additionally, transmission electron microscopy (TEM) observation is applied on the deformed specimens to examine their microscopic deformation mechanism. The TEM samples are prepared by ion bombardment thinning process and then the observation is performed on a high-resolution electron microscope JEM 2010.

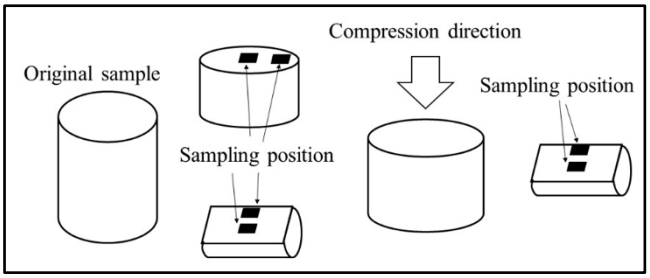

Fig.1 Schematic of compression sampling

2.3 Mechanical experiments

2.3.1 Specimens

Cylinder specimens of fully dense Ti-6Al-4V alloy with their axis parallel to the build direction are used for static and dynamic compression tests. The specimens are cut from the initially fabricated struts directly via wire cutting with a height-diameter ratio of 1.

Cubic micro-lattice specimens along the build direction are prepared directly through EBM and SLM for static compression tests. The micro-lattice structures comprise assembly of rhombic dodecahedron unit cells, which have been described in our previous study [33-35]. Table 2 exhibits the detail parameters of the fabricated lattice specimens, where the relative density ρ is calculated by $\rho=m/(v\rho_b)$. Here, m and v represent the mass and volume of the specimens respectively, ρ_b is the density of the bulk material. The strength of the micro-lattice structure can be simply determined by

$$\sigma_y = \frac{\sqrt{6}}{4}\sigma_{ys}\left(\frac{d}{l}\right)^3 = 0.21\sigma_{ys}\rho^{1.5} \quad (1)$$

where σ_{ys} is the yield strength of a single strut, d and l denote the diameter and length of a single strut respectively.

Table.2 Comparison of basic specifications between the two groups of specimens

Sample number	Designed dimensions(mm^3)	Actual dimensions(mm^3)	Mass(g)	Relative density	Fabrication method
1#	15^3	15.24× 15.2× 14.42	2.23	0.152	SLM

2#	15.23 × 15.22 × 14.39	2.27	0.155	EBM
3#	15.24 × 15.28 × 14.9	2.46	0.161	
4#	15.24 × 15.28 × 14.92	2.46	0.161	

2.3.2 Uniaxial compression testing procedure

Quasi-static compression experiments on the cylinder and cubic lattice specimens are carried out using the WDW-300 electronic universal testing machine. The loading processes are controlled by the movement of the upper indenter while the testing speed can be determined by the specimen height and a default strain rate of 1×10^{-3}/s. The loading force F during the testing process can be captured by the 300KN load cell, and the displacement δ of the incident can be recorded by the photoelectric encoder with a high resolution of 0.001mm and a low relative error of ±0.5%. Then the engineering stress-strain (σ_e-ε_e) and true stress-strain (σ-ε) relation of the dense materials could be obtained via

$$\begin{cases} \sigma_e = F/A_s \\ \varepsilon_e = \delta/l_s \end{cases} \text{ and } \begin{cases} \sigma = \sigma_e\left(1-\varepsilon_e\right) \\ \varepsilon = -\ln\left(1-\varepsilon_e\right) \end{cases} \tag{2}$$

where A_s and l_s represent the initial cross-section area and height of the specimens. For the testing of the micro-lattice specimens, a digital camera is adopted to capture the deformation evolution with a frame rate of 30fps.

2.3.3 Dynamic compression testing procedure

The dynamic compressive experiments are performed on a Split Hopkinson Pressure Bar (SHPB) system which has been commonly used for testing the dynamic behavior of materials at the strain rates ranging from 10^2~10^4/s. As shown in Fig.2, the SHPB apparatus consists of a striker, an incident bar and a transmission bar. All bars in the experiments are made of high strength maraging steel with a diameter of 13mm. The strikers are with two different lengths, namely, 300mm and 200mm respectively, while the incident and transmission bars are both 1000mm. The tested specimens are sandwiched between the incident and transmission bars. When the incident bar is impacted by the striker, a compressive stress pulse is generated at the interface and propagates toward the other end of the incident bar. The duration of the stress pulse t is associated with the length of the striker l and the sound speed of the bars C_0 by t=2l/ C_0. The stress pulse is divided into a tensile pulse which reflects back to the incident bar and a compressive pulse transmits to the output bar when it reaches the specimen section. During the loading process, all the bars remain elastic while the specimens deform plastically. Strain gages are located at the center of the incident and transmission bars to record the corresponding stress pulses. The signal is processed and amplified by a dynamic strain indicator, and recorded by an oscilloscope afterwards.

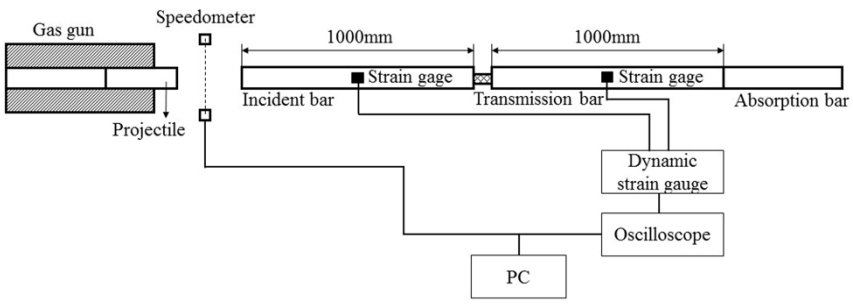

Fig.2 Schematic of SHPB apparatus

A basic assumption for SHPB testing is the equilibrium state at the bar-specimen interface, which indicates that

$$\left|\varepsilon_r(t)\right| + \varepsilon_t(t) = \varepsilon_i(t) \tag{3}$$

where $\varepsilon_i(t)$, $\varepsilon_r(t)$ and $\varepsilon_t(t)$ denote the incident wave, reflected wave and transmission wave obtained by the strain gages respectively. Then the dynamic engineering stress σ_e, strain ε_e and strain rate $\overset{\text{g}}{\varepsilon}$ can be derived according to the one-dimensional elastic wave theory as

$$\begin{cases} \overset{\text{g}}{\varepsilon} = -\dfrac{2C_0}{l_s}\varepsilon_r(t) \\ \varepsilon_e = \displaystyle\int_0^t \overset{\text{g}}{\varepsilon}\, d\tau \\ \sigma_e = \dfrac{E_B A_B}{A_s}\varepsilon_t(t) \end{cases} \tag{4}$$

here E_B and A_B are the elastic modulus and cross-section area of the bars respectively. Afterwards, the true stress σ and strain ε can be dealt with Eq.(2). A 100 point smoothing algorithm is applied to minimize the oscillation on the pulse signals recorded by the strain gages in the present manuscript. Fig.3 displays the typical curves after being processed to verify the equilibrium condition in our experiments. The related strain rates calculated by Eq.(4) are exhibited in Fig.4, which demonstrates that the strain rates during loading process, especially for those under low velocity impact are not constant. Thus, all the strain rates stated in this paper are determined as the rough average value during the plastic deformation process.

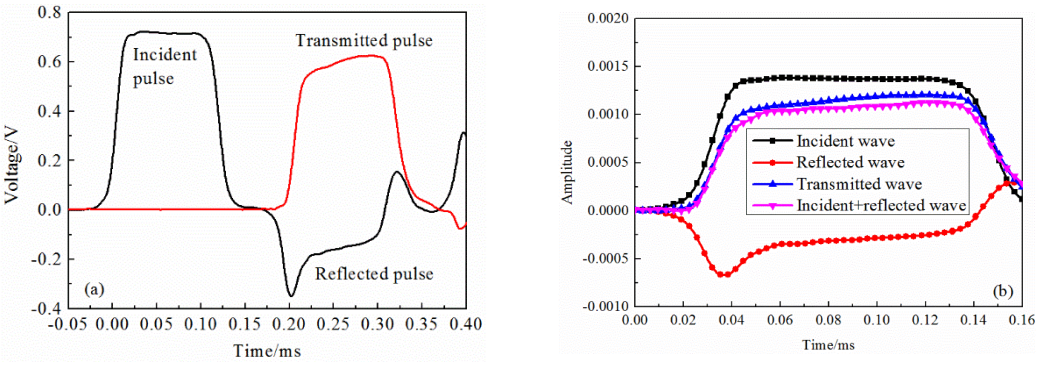

Fig.3 SHPB signals and calculated curves: (a) typical signals obtained from the strain gages; (b) wave-form separation figure for verifying the equilibrium condition

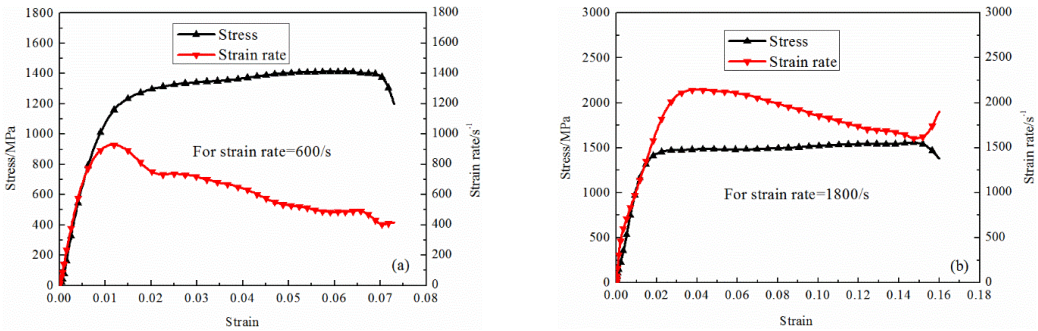

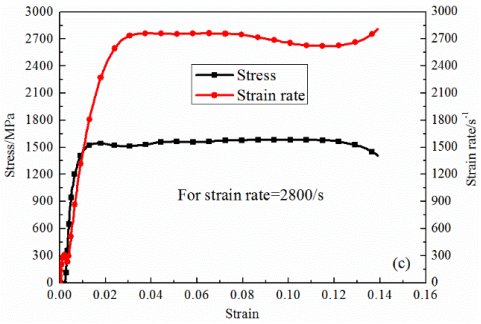

Fig.4 Imposed strain rate history corresponding to different strain rates

3 Results

3.1 Microstructural characterization of the printed materials

3.1.1 Cylinder dense specimen

As the additively-manufactured materials undergo very high cooling rates, the corresponding microstructure evolution is different from that processed by traditional methods. Fig.5(a)~(b) depicts the optical microstructure of EBM printed Ti-6Al-4V. It can be observed that the structure exhibits a typical basket weave pattern consists of α-lamina (white part) inside a β-phase (dark part) matrix. The images also present different grain arrangements at different locations in the specimens. Massive phase (circled by the red curve) is observed near the edge of the specimens which is absent at the specimen center. The massive phase grains have also been reported previously by Lu et.al.[22]. They attributed the formation of the massive phase to the low cooling rate of the EBM which led to the massive transformation. The optical microstructure of SLM printed Ti-6Al-4V is exhibited in Fig.5(c)~(d). The metallographic figures demonstrate that the microstructure of SLM parts is similar to that of EBM parts. Exactly, resulted from the fast cooling rates, the typical microstructure of Ti-6Al-4V obtained by SLM is martensitic (α') [12]. Due to the heat treatment after processing, the martensitic phase α' has decomposed to $\alpha+\beta$ phases, which makes the microstructure more similar to that of the EBM samples. Meanwhile, the microstructure in SLM parts is quite homogeneous at different locations as no massive phase has been detected. Moreover, the observation also implies that the materials printed by EBM and SLM method in the present study exhibit high density as nearly no micro-pores can be detected from the OM images.

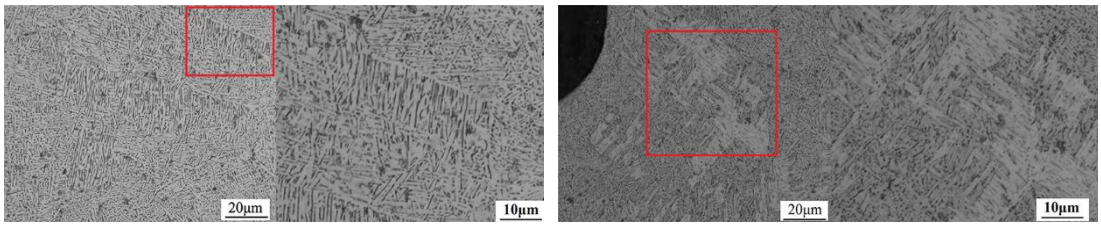

(a) (b)

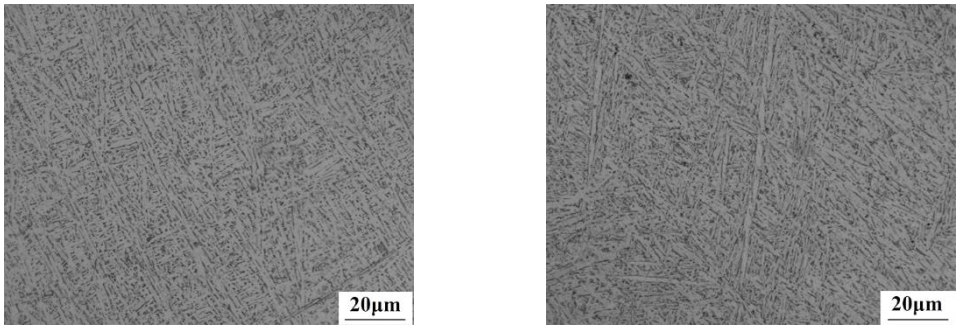

(c) (d)

Fig.5 Optical micrograph of additively-manufactured Ti-6Al-4V perpendicularly to the build direction: (a) at the center of EBM printed material; (b) near the edge of EBM printed material; (c) at the center of SLM printed material; (b) near the edge of SLM printed material (light phase = α, dark phase =β)

Fig.6 shows the scanning electron (SE) images of the EBM- and SLM-printed specimens, which can reflect the α+β dual phases with basket weave organization more apparently. The grain distributions and orientations of the additively-manufactured Ti-6Al-4V alloy are characterized by EBSD analysis. The representative maps of the [0001] HCP crystal plane orientation in Fig.7 apparently reflect a highly heterogeneous polycrystalline structure. Significant discrepancy in the texture between the struts fabricated by the two different approaches is concluded from the corresponding pole figures in Fig.7(c) and (d). In the EBM components, evident texture can be identified with Euler angles of (90°, 70°, 20°) and (90°, 70°, 75°), which also indicates that the material is anisotropic. This is related to the scanning strategy as the grains grow preferentially along the direction of powder stacking. The grain distribution in the SLM samples is similar to that of EBM parts. Nevertheless, the recrystallization annealing treatment may influence the texture of titanium alloy, which results in the nearly isotropic SLM strut as the texture is relatively weak.

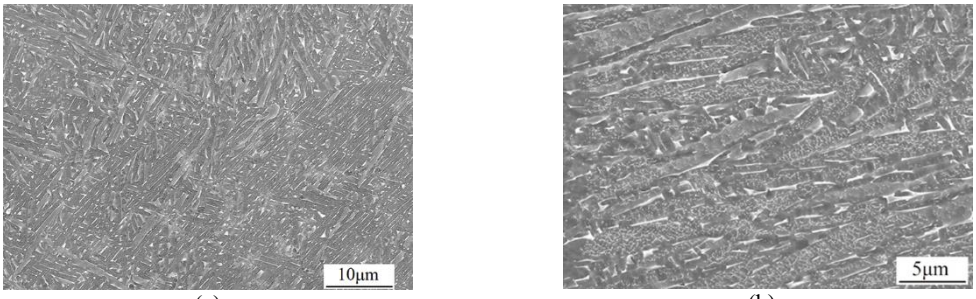

(a) (b)

Fig.6 SEM observations in the build direction on polished dense samples made by: (a) EBM; (b) SLM (dark phase = α, light phase =β)

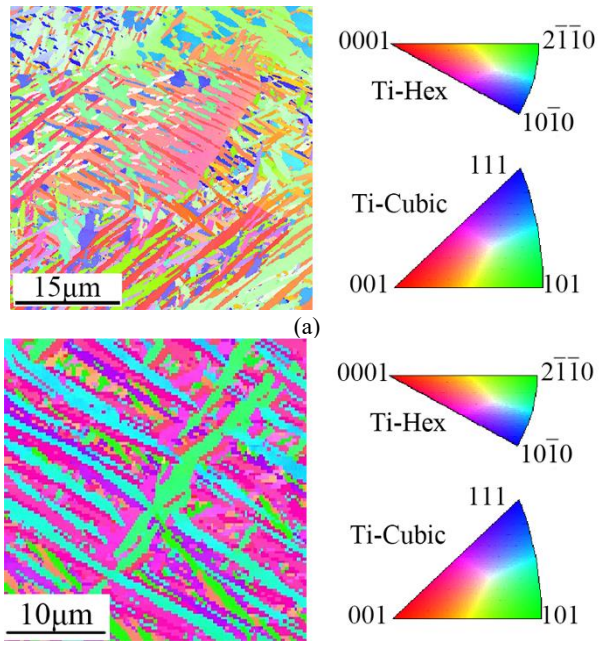

(a)

(b)

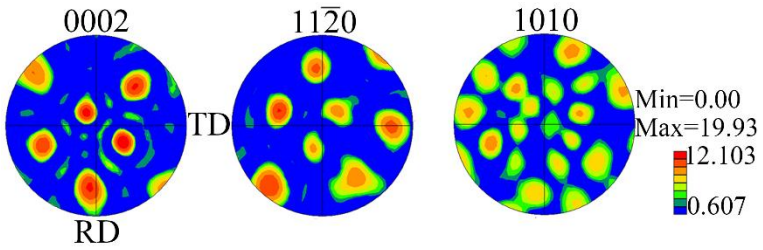

(c)

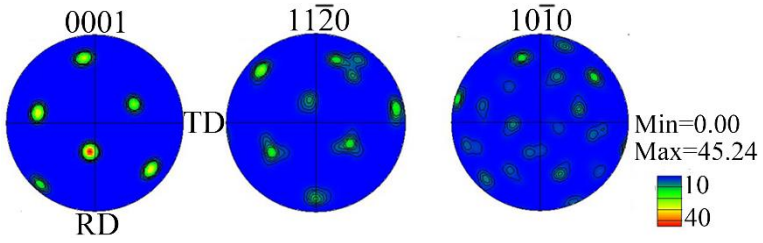

(d)

Fig.7 EBSD analysis of additively-manufactured Ti-6Al-4V alloy (Φ4mm × 4mm) in the build direction: (a) grain orientation map of EBM samples; (b) grain orientation map of SLM samples; (c) pole figures for EBM samples; (d) pole figures for SLM samples (all the data are measured at the center of the cross section)

The average α lamella sizes of the additively-manufactured Ti-6Al-4V are also measured during the EBSD analysis, which are plotted in Fig.8. The statistical data reveals that the SLM printed specimens with Φ4mm × 4mm possess smaller lamellas with an average value of 1.3μm as most sizes locate in 0.5~2.0μm (approximate 87%). For EBM printed materials with the same dimension, the fraction of lamellas larger than 2μm is about 45%, which leads to an average value of about 2.5μm. It can also be concluded from Fig.8(b) and Fig.8(d) that the lamellar size of EBM parts exhibit obvious size effect. The average grain size decreases from 2.50μm to 2.36μm with the component dimension shifting from Φ4mm × 4mm to Φ2mm × 2mm, which is caused by the higher cooling rate in the undersized struts [17]. For the SLM parts, the lamella size is slightly influenced by the part size (changing from 1.3μm to 1.33μm) due to the post heat-treatment.

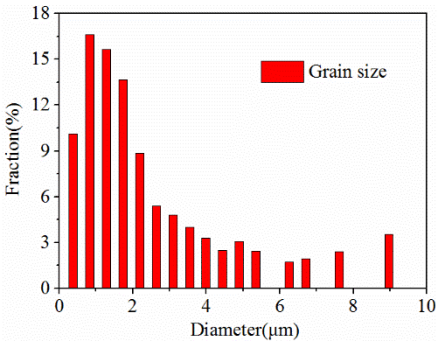

(a)

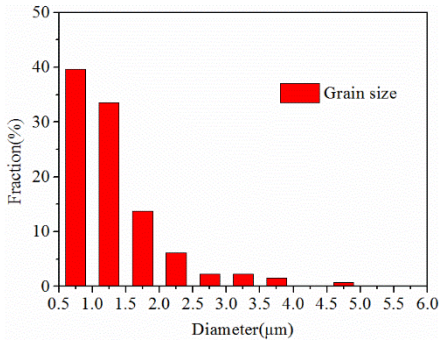

(b)

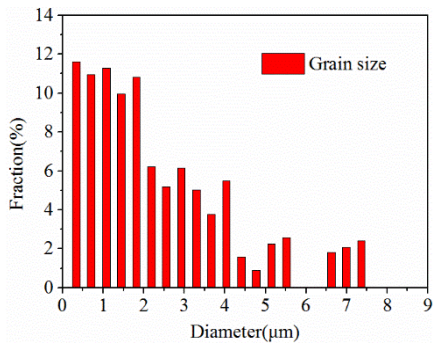

(c)

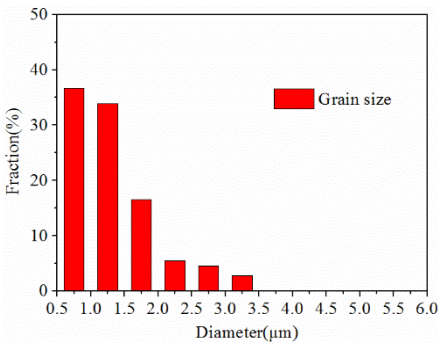

(d)

Fig.8 Grain size distribution of Ti-6Al-4V samples captured by EBSD: (a) with Φ4mm × 4mm printed by EBM; (b) with Φ4mm × 4mm printed by SLM; (c) with Φ2mm × 2mm printed by EBM; (b) with Φ2mm × 2mm printed by SLM (all the data are measured at the center of the cross section)

3.1.2 Cubic micro-lattice specimen

The perfect micro-lattice model used for fabrication is a cube comprised of 5 × 5 × 5 unit cells (15 × 15 × 15mm^3), but the measured specimen height is smaller than the in-plane dimensions, especially for the EBM-printed samples. The discrepancy leads to the deviation of relative density between the materials prepared by different processes. Fig.9 reveals the microstructure of the additively-manufactured micro-lattice structures and individual struts obtained by SEM observation. The images prove that the struts fabricated by EBM have complex structures with visible micro-defects such as varying diameters, non-molten powders and porosity. The poor surface quality can be influenced by the input energy. Low input energy leads to insufficient heating which results in unmelted powders and defects, while high input energy will induce balling caused by large surface tension of metal droplets generated from the melted powder. Some other factors such as slicing method and thickness of powder also affect the quality of fabrication. By contrast, the quality of specimens obtained from SLM is slightly better. However, the shape of all the struts manufactured by the two processes appear to deviate from the target shape which should be perfect cylinder.

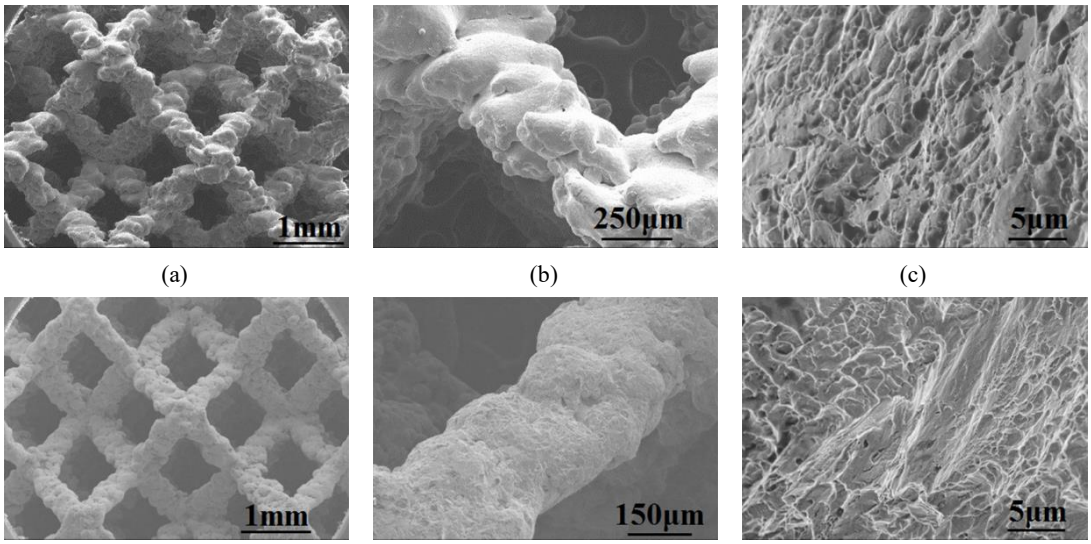

Fig.9 The SEM image of unpolished samples: (a) and (b) for the Ti-6Al-4V lattice structure and a single strut fabricated by EBM method; (d) and (e) for the Ti-6Al-4V lattice structure and a single strut fabricated by SLM method; (c) and (f) for the fracture surface morphology of struts fabricated by EBM and SLM method respectively

3.2 Stress-strain response of the dense materials

The true stress-strain curves of the bulk Ti-6Al-4V alloy obtained from static and dynamic compression experiments on the middle size specimens (Φ4mm × 4mm) are depicted in Fig.10. It can be observed that both the printed materials exhibit the strain rate sensitivity. The measured quasi-static yield strength at 0.2% plastic strain of EBM-printed Ti-6Al-4V alloy is about 863MPa, which is elevated to 1080MPa and 1156MPa under strain rates of 1500/s and 3000/s respectively. For the SLM-printed specimens, the yield strength are 935MPa, 1134MPa and 1453MPa under strain rates of 0.001/s, 1300/s and 3000/s respectively. The results indicate that the SLM-printed dense materials exhibit higher strength than the EBM-printed specimens. Besides, the SLM parts also appear to be more sensitive to strain rate when elevated from 0.001/s to 3000/s. The results also reveal that the EBM parts feature a hardening modulus of 1346MPa over the strain interval [0.05, 0.15] under quasi-static compression, which turns to 86MPa under a strain rate of 1500/s. When the

strain rate is elevated to 3000/s, the EBM-printed sample is totally softened due to the thermal effect and the failure of the material. It is noted that even though the same alloy the SLM parts present a distinct hardening behavior. The related hardening modulus almost keeps unchanged (1699MPa and 1492MPa) when compressed from 0.001/s to 1300/s, and decreases to 700MPa under a strain rate of 3000/s.

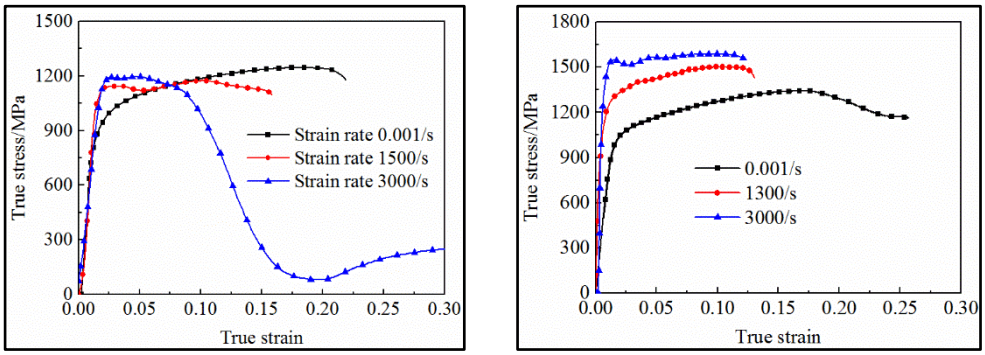

Fig.10 Dynamic compressive stress-strain curves of Ti-6Al-4V alloy with Φ4mm×4mm: (a) printed by EBM; (b) printed by SLM

Fig.11 summaries the yield strength of the 3D-printed dense struts with different dimensions and strain rates. The results denote that the SLM printed struts exhibit superior strength over the EBM fabricated ones with various dimensions. For the EBM parts, evident decline in the strength can be captured when the specimen size is below 4mm, which signifies that the compressive behavior of the EBM components present size sensitivity. For the SLM parts, the size effect on the material strength is relatively slight. The results also suggest that both of the two method processed materials display apparent strain rate sensitivity, but some differences should be noted. For the EBM parts, the strength enhancement is not significant when the strain rate is below 1000/s. The amplification is about 5% when the strain rate is elevated from 0.001/s to 800/s for the EBM fabricated struts. When the strain rate is higher than 1000/s, the strength of the material increases sharply. By contrast, the SLM parts are more sensitive to the strain rate.

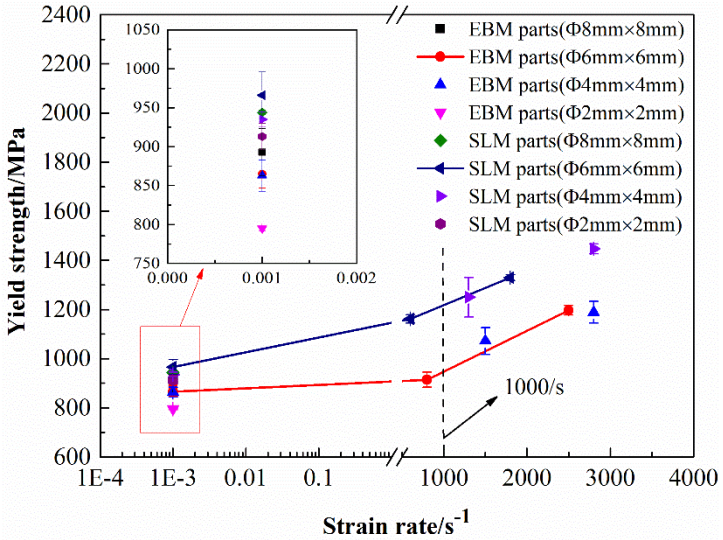

Fig.11 Yield strength of 3D printed struts with dimensions ranging from Φ2mm×2mm to Φ8mm×8mm under different strain rates

3.3 Stress-strain response of the micro-lattice materials

Fig.12 shows the quasi-static compressive stress-strain curves of Ti-6Al-4V lattice materials fabricated by EBM and SLM respectively. The different stress-strain curves exhibit similar patterns which can be divided into three regions. Firstly, the stress increases linearly with the strain as the struts undergo elastic deformation. Afterwards, a plateau stress region emerges where the struts enter the plastic deformation. Finally, the stress increases rapidly when all the struts are compacted together and the lattice materials behave as bulk solids. Significant reduction can be observed in both EBM and SLM curves after the initial peak stress.

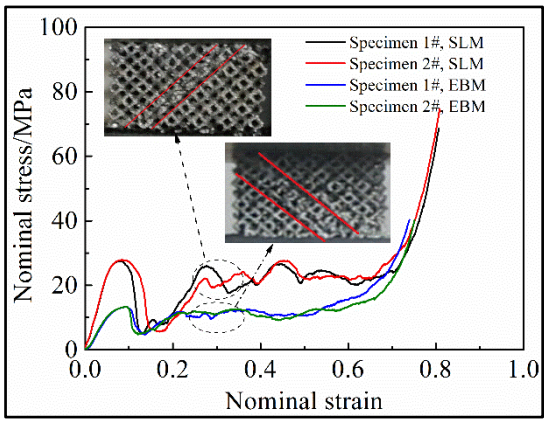

Fig.12 Quasi-static stress-strain curves of printed Ti-6Al-4V micro-lattice structures

Fig.12 also presents the deformation modes of the lattice specimens with a nominal strain of 0.3. It can be noted that both of the specimens fabricated by different methods deformed in a same pattern. Visible localization resulted from the yielding and fracture of struts emerged along the 45° direction in the lattice structures. The localization was quite similar to the shear band in isotropic solids subjected to uniaxial compression. Cheng.et.al [30] has explained the crush band in this lattice structure according to the force analysis on rhombic dodecahedron unit cell. The experimental results demonstrated that the deformation mechanism of rhombic dodecahedron Ti-6Al-4V lattice structure had not been affected by the two different manufacture process.

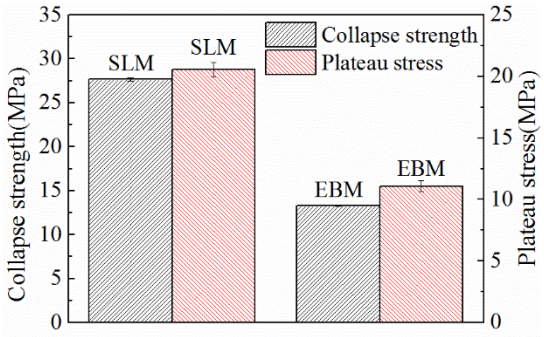

(a)

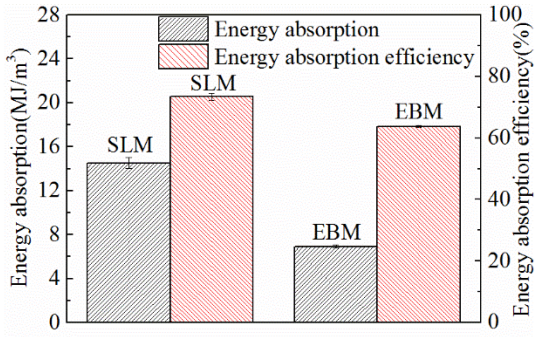

(b)

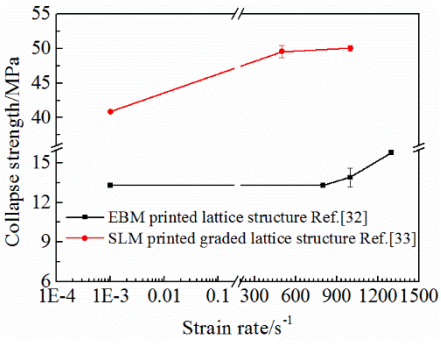

(c)

Fig.13 Mechanical properties of printed Ti-6Al-4V micro-lattice structures: (a) quasi-static strength and plateau stress; (b) energy absorption performance; (c) dynamic strength

Aiming at judging the discrepancy between the two preparation procedures, collapse strength and plateau stress are chosen for comparison as exhibited in Fig.13(a). Collapse strength is defined as the first peak stress which can reflect the load capacity of structure, while plateau stress is an important parameter to evaluate the energy absorption capacities of the cellular materials. It can be easily concluded that the collapse strength and plateau stress of the SLM manufactured Ti-6Al-4V lattice structures are almost twice as much as those of the EBM components. Consequently, the energy absorption characteristics of the specimens prepared by SLM is also more excellent than those of EBM parts (Fig.13(b)). The dynamic response of the same EBM-printed Ti-6Al-4V micro-lattice structures has been investigated in our previous study[34]. The corresponding dynamic collapse strengths are plotted in Fig.13(c), which indicates that the micro-lattice structures are also sensitive to strain rate. Similar to the dense material (Φ6mm × 6mm) in Fig.11, the dynamic strengths of the lattice structures present a two-stage variation. The rate sensitivity is not obvious when the strain rate is below1000/s and turns to be more apparent with the increase of strain rate. Although the dynamic behavior of the SLM-printed micro-lattice structures has not been tested, the related experiments have been performed on the graded samples with the same cells and fabrication process[35]. The collapse strengths depicted in Fig.13(c) demonstrate that the SLM components are more sensitive to strain rate than the EBM processed specimens, which is accordance with the trend of the dense material in Fig.11.

4 Discussions

Our research has revealed that the mechanical properties of the prototype bulk material vary substantially with different fabrication approaches. The comparison between the EBM-made and SLM-made dense specimens demonstrates that the difference in processing methods can result in a yield strength difference of almost 10%. The comparison for the lattice structures are in line with the results from the dense material, which reveals that the two different fabrication processes can lead to differences in the collapse strength and plateau stress of about 50%. The results also indicate that with the decrease in specimen size, the discrepancy between the materials manufactured by the two fabrication approaches becomes more apparent. The above discrepancy may be caused by the different microstructure and geometric defects in the printed materials treated by different processes, which will be discussed in this section.

4.1 The effect of microstructure on the mechanical properties

The microstructure of crystalline materials is significantly related to their mechanical properties. It has been displayed in Fig.8 that the lamellar size distributions of EBM-made and SLM-made material are quite different. The lamellar spacing of EBM-printed material is sensitive to the part size, while the SLM-printed material is not. According to Hall-Petch relation [38,39], the strength of crystalline metal materials can be evaluated by the lamellar spacing as:

$$\sigma_y = \sigma_0 + kd^{-1/2} \tag{5}$$

where σ_y is the yield strength of the material, σ_0 is the yield strength of the corresponding single

crystal material, *d* represents the average grain size (or lamellar spacing) and *k* the constant. For the same material, the yield strength can be significantly affected by the grain size which can be quantified by the *k* value. By following an approximate Hall-Petch relationship, the mechanical properties of lamellar Ti-6Al-4V has been reported to be improved with the lamellar spacing decreases[40]. The literature data [6, 40-47] as well as the present data on yield strength vs. the inverse square root of α lamellar spacing for Ti-6Al-4V is plotted in Fig.14. The image demonstrates that most of the data satisfies the Hall-Petch relationship, and the yield strengths obtained in the present study also match well with this relationship. Consequently, the coarse-lamella results in the lower strengths of EBM-part compared with the specimens fabricated by SLM process. Meanwhile, the yield strength of SLM-part nearly keeps unchanged with the part size decreases as the *α* lamellar spacing is similar.

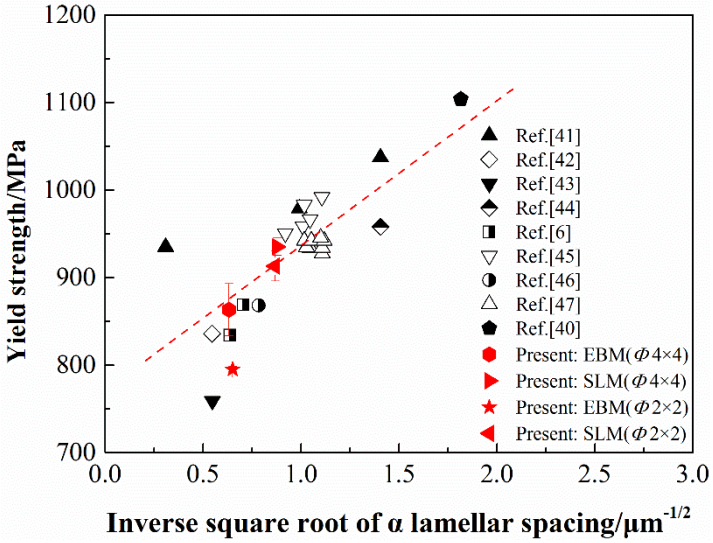

Fig.14 Yield strength vs. the inverse square root of *α* lamellar spacing for Ti-6Al-4V

4.2 The effect of geometric defects on the mechanical properties

Although comparison between the SLM-printed and EBM-printed parts with *Φ*4mm×4mm exhibits that the yield strength is analogous to the Hall-Petch relationship, it should be noted that the strength of EBM parts decreases significantly when the specimen is smaller than *Φ*4mm×4mm. The average lamellar spacing shown in Fig.8 decreases from 2.50μm to 2.36μm with the EBM-component getting smaller from *Φ*4mm×4mm to *Φ*2mm×2mm, which should result in the elevation of yield strength according to the Hall-Petch relation. The contradiction between the experimental data and the theoretical prediction is considered to be resulted from the geometric irregularity. With the diameter of the EBM printed strut decreases, the shape of transverse cross section tends to be more irregular which may produce imperfections on the surface and reduce the material properties. More apparent geometric defects such as strut waviness, strut thickness variation and strut oversizing or undersizing are reflected from EBM struts as shown in Fig.9. Although some micro-defects can also be observed on the SLM struts, the extent of strut thickness variation is much lower than that of EBM struts. Liu et.al. [48] found that the compressive strength of lattice structures is very sensitive to the imperfections including strut waviness and especially for strut thickness variation, which means that the strength of EBM lattice structures will be lower than that of SLM

lattice structures.

Another type of defect should be taken into consideration is the surface roughness. Compared with the SLM-made struts, the EBM struts exhibit much rougher surface caused by the sintered particles during the pre-heating process which cannot be removed during the powder-blowing process. The different surface roughness can be easily identified from Fig.16. These powders only increase the diameter of the struts but cannot contribute to their load bearing capacity. Thus, the rough layer near the surface should be considered as mechanically inefficient and the percentage of the inefficient part is larger for the slenderer strut. Therefore, the yield strength of EBM-printed struts decreases sharply when the diameter is smaller than 4mm. The collapse strength of the EBM lattice structures is much lower than that of the SLM-printed structures as well although their relative densities are quite close. The effect of surface finish on the yield strength has been demonstrated by Formanoir et.al [23]. In their study, the area of the inefficient region was removed when they calculated the stress-strain curves of the EBM-printed specimens, and the results matched well with those of the polished specimens. In addition, they also concluded that the mechanical performance of the lattice structure could be promoted by chemical etching as the surface roughness was significantly improved [24]. Wang et.al. [49] also reported that the part size had an obvious effect on the tensile properties of EBM Ti-6Al-4V specimens when the diameter was less than 4mm, nevertheless, their specimens were well polished before experiment which led to the conclusions contrary to our results.

4.3 Failure mechanism of the printed materials

The fracture characteristics and mechanisms of the AM materials are identified by OM and SEM/TEM observations on the deformed specimens. An arc-shaped shear band can be observed from the top view of both the SLM and EBM printed samples (Fig.15(a)). Fig.15(b) demonstrates that the fracture in the specimens occurred along the plane inclined at an angle of 45° plane to the compression axis. Such failure modes are observed during both quasi-static and dynamic compressive deformations. This fracture mechanism has been explained by Ran et.al. [50] in their investigation on the fracture behavior of Ti-55511 alloy. As shown in Fig.15(c), localized shear bands emerge on the 45° plane to the axis of compression corresponding to the maximum shear stress orientation when uniaxial loaded. Meanwhile, a hoop stress is generated at the equatorial plane of the cylindrical surface when a bulge exists on the specimen, which leads to a tensile loading state. The above stress states result in the coexistence of tension-shear-compression region (denoted as 1) and shear-compression region (denoted as 2) in the fracture surfaces [50]. Similar phenomenon has also been reported by Lee end Lin [51]. It should also be noted that due to the border effect (friction between sample surface with the platens of the machining test), the fracture started at the surface in contact with the rigid platen. This can be avoided by adjusting the size of the specimen, for which the height of the sample should be 1.5~2 times its diameter.

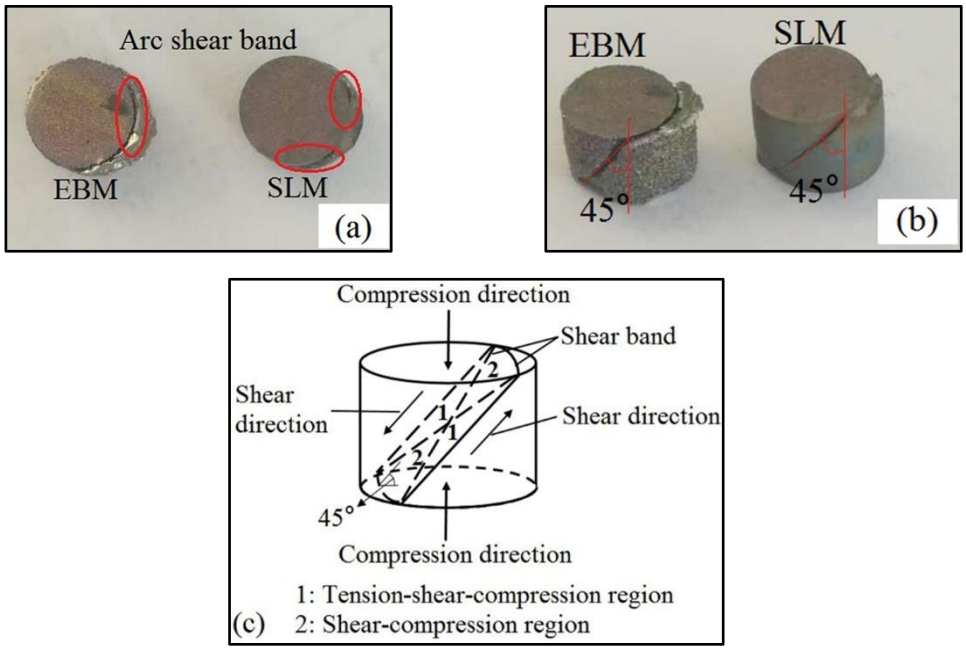

Fig.15 (a) Top view of the deformed additively manufactured specimens; (b) Side view of the deformed samples; (c) Schematic of the fracture characteristics and orientation of shear band of additively manufactured Ti-6Al-4V alloy under compression

As the EBM parts exhibit obvious size effect on the macroscopic mechanical properties, the microstructure on the fracture surface with different sample dimensions also captured our interest. Fig.16 shows the typical fracture morphology of EBM manufactured Ti-6Al-4V alloy with Φ4mm×4mm and Φ2mm×2mm under quasi-static compression loading (0.001/s). Apparent parabolic dimples elongated along the shear direction can be observed in both specimens, which indicates that the specimens undergo large plastic deformations. As shown in Fig.16(b) and Fig.16(d), the larger size and depth of the parabolic dimples in the specimens with Φ2mm×2mm than those in the specimens with Φ4mm 4mm verifies that the ductility of the EBM parts increases with the enhancement of the specimen size. It can also be observed from Fig.16(c) that apparent boundary exists in the smaller specimens. It can also be concluded that the ductility of the SLM components needs to be improved as the dimples are shallower than those of the EBM parts. This is also supported by the observation on the micro-lattice struts shown in Fig.9(c) and (e).

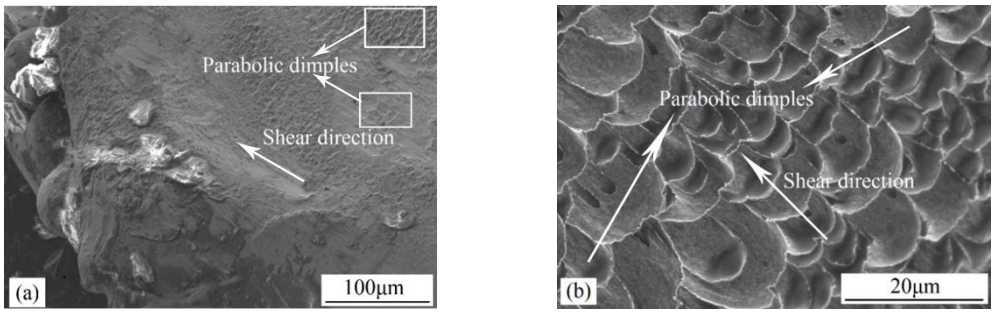

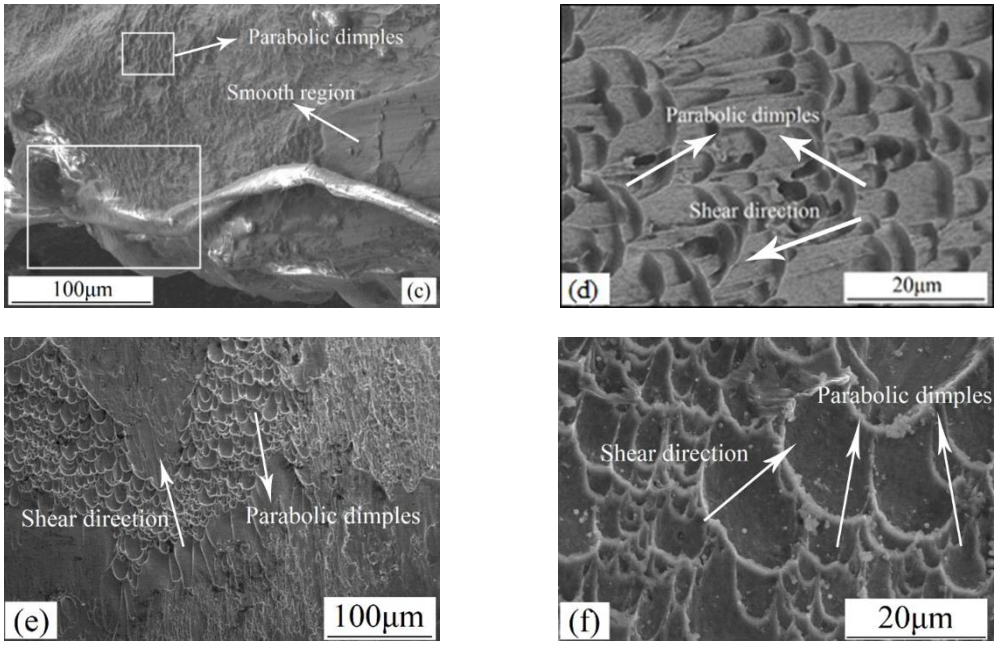

Fig.16 Typical fracture morphologies of additively-manufactured parts: (a) and (b) for EBM parts with Φ4mm × 4mm; (c) and (d) for EBM parts with Φ2mm × 2mm; (e) and (f) for SLM parts

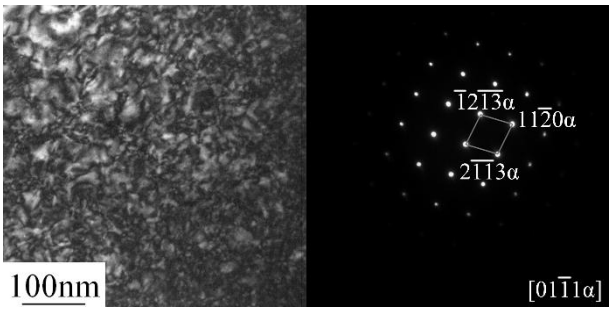

(a)

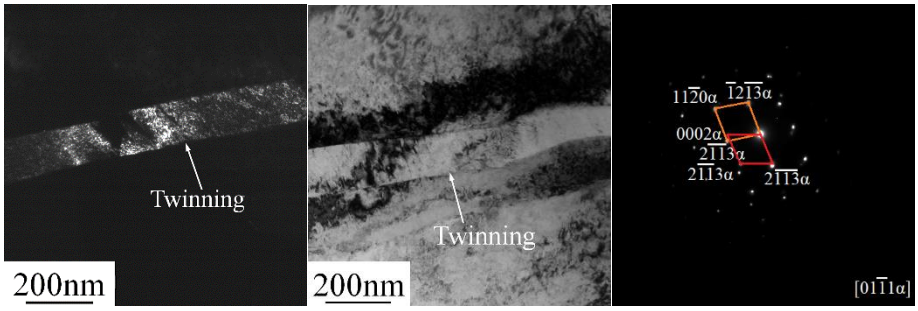

(b)

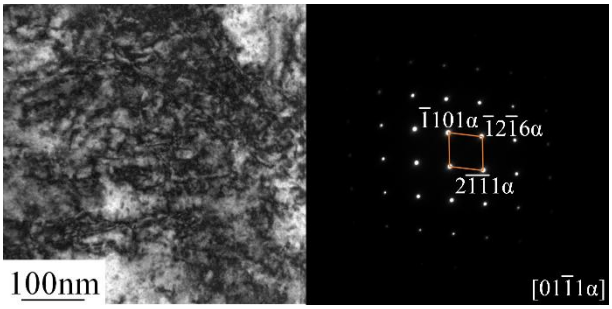

(c)

Fig.17 Microscopic deformation mechanism of additively manufactured Ti-6Al-4V: (a) and (b) for EBM parts; (c) for SLM parts

Fig.17 exhibits the TEM observations on the deformed samples subjected to compressive loadings. The images indicate that large amounts of dislocations appear in both EBM and SLM printed materials. Nevertheless, twinning is also captured in the struts fabricated by EBM, which is absent in the SLM struts. Consequently, the lower active stress of twinning leads to a lower yield strength of EBM struts. Usually, the emergence of twinning will become the barrier to dislocation movement which leads to the hardening on the post-yielding behavior of the material. But it seems to have limit influence on the hardening of the EBM fabricated material since the twinning density is relatively low. In addition, the emergency of twinning may also contribute to the ductility of the material. For the hcp crystals, the slip systems are quite few which make the slip difficult. Twinning can coordinate grain deformation which makes the previously unfavorable slip systems shift to favorable positions, then the slip deformation will continue to obtain a higher deformation. It has also been stated by Zhang et.al [52] that the twinning can provide pathways for the easy motion of dislocations which leads to the larger deformation than the material without twinning.

5 Conclusions

The compressive behavior of additively-manufactured titanium alloy and its micro-lattice structures is investigated via experiments. Two fabrication processes including EBM and SLM are taken into consideration. Electronic testing machine is used for quasi-static tests and higher loading velocities are performed by using SHPB. Microstructural characterization is conducted by metallographic observation and EBSD analysis. The influences of different fabrication processes and part sizes on the mechanical properties of Ti-6Al-4V are revealed. Some conclusions have been drawn as follows:

(1) Comparing with the EBM printed Ti-6Al-4V struts and micro-lattice structures, the SLM printed parts exhibit higher strength. Nevertheless, the failure mechanism of the specimens is not affected by the fabrication method.

(2) The EBM parts exhibit apparent size sensitivity as the mechanical performance is largely reduced when the specimen size is smaller than 4mm. But the size effect can be ignored in the SLM parts.

(3) The geometric irregularities is attributed to the reduction of the material strength. The surface irregularities of the EBM samples are more significant than those found in the SLM samples. This deleterious effect is greater with the sample size decreases, which results in the large

discrepancy between the mechanical behavior of the lattice structures fabricated by these two approaches.

(4) The EBM parts are anisotropic as apparent texture can be captured, while the SLM components tend to be isotropic. The TEM observation indicates that twinning appears in the deformed EBM parts which is absent in the SLM struts.

(5) The strengths of the EBM parts are not sensitive to the strain rate below 1000/s, while the sensitivity becomes apparent when the strain rate is above this value. However, the strain rate sensitivity of the SLM parts keeps identical with the strain rate varies. This phenomenon needs to be further investigated in our subsequent study.

Acknowledgements:

The author acknowledges the financial support of the National Natural Science Foundation of China (11672043, 11802028), the Project funded by China Postdoctoral Science Foundation (2018M640072), the National Key R&D Program of China (2016YFC0801200), the Opening Project of State Key Laboratory of Traction Power (TPL1701), the Project of State Key Laboratory of Explosion Science and Technology (YBKT18-07), the Graduate Technological Innovation Project of Beijing Institute of Technology (2017CX10013) and other projects of China (6140922020116BQ01002, 614260601010617 and SAST2017-029).

References:

[1] R. Boyer, G. Welsch, E.W. Colilngs, Materials Properties Handbook: Titanium Alloys, 1994. doi:http://www.sciencedirect.com/science/article/pii/S0045782504000313.

[2] A. Majorell, S. Srivatsa, R.C. Picu, Mechanical behavior of Ti-6Al-4V at high and moderate temperatures-Part I: Experimental results, Mater. Sci. Eng. A. 326 (2002) 297-305. https://doi.org/10.1016/S0921-5093(01)01507-6.

[3] C.G. Rhodes, N.E. Paton, Formation characteristics of the α/β interface phase in Ti-6Al-4V, Metall. Trans. A 10 (1979) 209-216. https://doi.org/10.1007/BF02817630.

[4] H.K. Rafi, N.V. Karthik, H. Gong, T.L. Starr, B.E. Stucker, Microstructures and mechanical properties of Ti6Al4V parts fabricated by selective laser melting and electron beam melting, J. Mater. Eng. Perform. 22 (2013) 3872-3883. https://doi.org/10.1007/s11665-013-0658-0

[5] J.P. Kruth, G. Levy, F. Klocke, T.H.C. Childs, Consolidation phenomena in laser and powder-bed based layered manufacturing, CIRP Ann. - Manuf. Technol. 56 (2007) 730-759. https://doi.org/10.1016/j.cirp.2007.10.004.

[6] L.E. Murr, S.A. Quinones, S.M. Gaytan, M.I. Lopez, A. Rodela, E.Y. Martinez, D.H. Hernandez, E. Martinez, F. Medina, R.B. Wicker, Microstructure and mechanical behavior of Ti-6Al-4V produced by rapid-layer manufacturing, for biomedical applications, J. Mech. Behav. Biomed. Mater. 2 (2009) 20-32. https://doi.org/10.1016/j.jmbbm.2008.05.004.

[7] L. Thijs, F. Verhaeghe, T. Craeghs, J. Van Humbeeck, J.P. Kruth, A study of the microstructural evolution during selective laser melting of Ti-6Al-4V, Acta Mater. 58 (2010) 3303-3312. https://doi.org/10.1016/j.actamat.2010.02.004.

[8] L. Facchini, E. Magalini, P. Robotti, A. Molinari, S. Höges, K. Wissenbach, Ductility of a Ti-6Al-4V alloy produced by selective laser melting of prealloyed powders, Rapid Prototyp. J. 16 (2010) 450-459. https://doi.org/10.1108/13552541011083371.

[9] H. Attar, M. Calin, L.C. Zhang, S. Scudino, J. Eckert, Manufacture by selective laser melting and mechanical behavior of commercially pure titanium, Mater. Sci. Eng. A. 593 (2014) 170-177. doi:10.1016/j.msea.2013.11.038.

[10] E. Chlebus, B. Kuźnicka, T. Kurzynowski, B. Dybala, Microstructure and mechanical behaviour of Ti-6Al-7Nb alloy produced by selective laser melting, Mater. Charact. 62 (2011) 488-495. https://doi.org/10.1016/j.matchar.2011.03.006.

[11] M. Simonelli, Y.Y. Tse, C. Tuck, Effect of the build orientation on the mechanical properties and fracture modes of SLM Ti-6Al-4V, Mat. Sci. Eng. A 616 (2014) 1-11. https://doi.org/10.1016/j.msea.2014.07.086.

[12] Khorasani A M, Gibson I, Awan U S, et al. The effect of SLM process parameters on density, hardness, tensile strength and surface quality of Ti-6Al-4V. Addit. Manuf. 25 (2019) 176-186.

[13] B. Vrancken, L. Thijs, J.P. Kruth, J.V. Humbeeck, Heat treatment of Ti6Al4V produced by Selective Laser Melting: Microstructure and mechanical properties, J. Alloy Compd. 541 (2012) 177-185. https://doi.org/10.1016/j.jallcom.2012.07.022.

[14] C. Qiu, N.J.E. Adkins, M.M. Attallah, Microstructure and tensile properties of selectively laser-melted and of HIPed laser-melted Ti–6Al–4V, Mat. Sci. Eng. A 578 (2013) 230-239. https://doi.org/10.1016/j.msea.2013.04.099.

[15] J. Yang, H. Yu, J. Yin, M. Gao, Z. Wang, X. Zeng, Formation and control of martensite in Ti-6Al-4V alloy produced by selective laser melting, Mater. Des. 108 (2016) 308-318. https://doi.org/10.1016/j.matdes.2016.06.117.

[16] M.F. Zäh, S. Lutzmann, Modelling and simulation of electron beam melting, Prod. Eng. 4 (2010) 15-23. https://doi.org/10.1007/s11740-009-0197-6.

[17] N. Hrabe, T. Quinn, Effects of processing on microstructure and mechanical properties of a titanium alloy (Ti-6Al-4V) fabricated using electron beam melting (EBM), Part 1: Distance from build plate and part size, Mat. Sci. Eng. A, 573 (2013) 264-270. https://doi.org/10.1016/j.msea.2013.02.064.

[18] N. Hrabe, T. Quinn, Effects of processing on microstructure and mechanical properties of a titanium alloy (Ti – 6Al – 4V) fabricated using electron beam melting (EBM), Part 2: Energy input, orientation, and location, Mat. Sci. Eng. A 573 (2013) 271-277. https://doi.org/10.1016/j.msea.2013.02.065.

[19] S.S. Al-Bermani, M.L. Blackmore, W. Zhang, I. Todd, The origin of microstructural diversity, texture, and mechanical properties in electron beam melted Ti-6Al-4V, Metall. Mater. Trans. A Phys. Metall. Mater. Sci. 41 (2010) 3422-3434. https://doi.org/10.1007/s11661-010-0397-x.

[20] X. Tan, Y. Kok, Y.J. Tan, M. Descoins, D. Mangelinck, S.B. Tor, K.F. Leong, C.K. Chua, Graded microstructure and mechanical properties of additive manufactured Ti-6Al-4V via electron beam melting, Acta Mater. 97 (2015) 1-16. https://doi.org/10.1016/j.actamat.2015.06.036.

[21] L.E. Murr, E. V. Esquivel, S.A. Quinones, S.M. Gaytan, M.I. Lopez, E.Y. Martinez, F. Medina, D.H. Hernandez, E. Martinez, J.L. Martinez, S.W. Stafford, D.K. Brown, T. Hoppe, W. Meyers, U. Lindhe, R.B. Wicker, Microstructures and mechanical properties of electron beam-rapid manufactured Ti-6Al-4V biomedical prototypes compared to wrought Ti-6Al-4V, Mater. Charact. 60 (2009) 96-105. https://doi.org/10.1016/j.matchar.2008.07.006.

[22] S.L. Lu, M. Qian, H.P. Tang, M. Yan, J. Wang, D.H. StJohn, Massive transformation in Ti-6Al-4V additively manufactured by selective electron beam melting, Acta Mater. 104 (2016) 303-

311. https://doi.org/10.1016/j.actamat.2015.11.011.
[23] C.D. Formanoir, S. Michotte, O. Rigo, L. Germain, S. Godet. Electron beam melted Ti–6Al–4V: Microstructure, texture and mechanical behavior of the as-built and heat-treated material. Mater. Sci. Eng. A, 652 (2016) 105-119.
[24] C.D. Formanoir, M. Suard, R. Dendievel, G. Martin, S. Godet. Improving the mechanical efficiency of electron beam melted titanium lattice structures by chemical etching. Addit. Manuf. 11 (2016) 71-76.
[25] P. Lhuissier, C.D. Formanoir, G. Martin, R. Dendievel, S. Godet. Geometrical control of lattice structures produced by EBM through chemical etching: Investigations at the scale of individual struts. Mater. Des. 110 (2016) 485-493.
[26] R.A.W. Mines, S. Tsopanos, Y. Shen, R. Hasan, S.T. McKown, Drop weight impact behaviour of sandwich panels with metallic micro lattice cores, Int. J. Impact Eng. 60 (2013) 120-132. https://doi.org/10.1016/j.ijimpeng.2013.04.007.
[27] E. Sallica-Leva, A.L. Jardini, J.B. Fogagnolo, Microstructure and mechanical behavior of porous Ti-6Al-4V parts obtained by selective laser melting, J. Mech. Behav. Biomed. Mater. 26 (2013) 98-108. https://doi.org/10.1016/j.jmbbm.2013.05.011.
[28] T. Tancogne-Dejean, A.B. Spierings, D. Mohr, Additively-manufactured metallic micro-lattice materials for high specific energy absorption under static and dynamic loading, Acta Mater. 116 (2016) 14-28. https://doi.org/10.1016/j.actamat.2016.05.054.
[29] S.J. Li, L.E. Murr, X.Y. Cheng, Z.B. Zhang, Y.L. Hao, R. Yang, F. Medina, R.B. Wicker, Compression fatigue behavior of Ti-6Al-4V mesh arrays fabricated by electron beam melting, Acta Mater. 60 (2012) 793-802. https://doi.org/10.1016/j.actamat.2011.10.051.
[30] X.Y. Cheng, S.J. Li, L.E. Murr, Z.B. Zhang, Y.L. Hao, R. Yang, F. Medina, R.B. Wicker, Compression deformation behavior of Ti-6Al-4V alloy with cellular structures fabricated by electron beam melting, J. Mech. Behav. Biomed. Mater. 16 (2012) 153-162. https://doi.org/10.1016/j.jmbbm.2012.10.005.
[31] S.J. Li, Q.S. Xu, Z. Wang, W.T. Hou, Y.L. Hao, R. Yang, L.E. Murr, Influence of cell shape on mechanical properties of Ti-6Al-4V meshes fabricated by electron beam melting method, Acta Biomater. 10 (2014) 4537-4547. https://doi.org/10.1016/j.actbio.2014.06.010.
[32] S. Li, S. Zhao, W. Hou, C. Teng, Y. Hao, Y. Li, R. Yang, R.D.K. Misra, Functionally Graded Ti-6Al-4V Meshes with High Strength and Energy Absorption, Adv. Eng. Mater. 18 (2016) 34-38. https://doi.org/10.1002/adem.201500086.
[33] L. Xiao, W. Song, C. Wang, H. Liu, H. Tang, J. Wang, Mechanical behavior of open-cell rhombic dodecahedron Ti-6Al-4V lattice structure, Mater. Sci. Eng. A. 640 (2015) 375-384. https://doi.org/10.1016/j.msea.2015.06.018.
[34] L. Xiao, W. Song, C. Wang, H. Tang, Q. Fan, N. Liu, J. Wang, Mechanical properties of open-cell rhombic dodecahedron titanium alloy lattice structure manufactured using electron beam melting under dynamic loading, Int. J. Impact Eng. 100 (2017) 75-89. https://doi.org/10.1016/j.ijimpeng.2016.10.006.
[35] L. Xiao, W. Song, Additively-manufactured functionally graded Ti-6Al-4V lattice structures with high strength under static and dynamic loading: Experiments, Int. J. Impact Eng. 111 (2018) 255-272. https://doi.org/10.1016/j.ijimpeng.2017.09.018.
[36] J. Parthasarathy, B. Starly, S. Raman, A. Christensen, Mechanical evaluation of porous titanium (Ti6Al4V) structures with electron beam melting (EBM), J. Mech. Behav. Biomed. Mater. 3

(2010) 249. https://doi.org/10.1016/j.jmbbm.2009.10.006.
[37] S.M. Gaytan, L.E. Murr, E. Martinez, J.L. Martinez, B.I. MacHado, D.A. Ramirez, F. Medina, S. Collins, R.B. Wicker, Comparison of microstructures and mechanical properties for solid and mesh cobalt-base alloy prototypes fabricated by electron beam melting, Metall. Mater. Trans. A 41 (2010) 3216-3227. https://doi.org/10.1007/s11661-010-0388-y.
[38] E.O. Hall, The deformation and ageing of mild steel III Discussion of results\t, Proc. Phys. Soc. Sect. B. 64 (1951) 495. https://doi.org/10.1088/0370-1301/64/9/303.
[39] N.J. Petch, The cleavage strength of polycrystals, J. Iron Steel Inst. 174 (1982) 25-28. https://doi.org/10.1007/BF01972547.
[40] W. Xu, M. Brandt, S. Sun, et al. Additive manufacturing of strong and ductile Ti–6Al–4V by selective laser melting via in situ martensite decomposition. Acta Mater. 85 (2015) 74-84. https://doi.org/10.1016/j.actamat.2014.11.028.
[41] B. Baufeld, O. Van Der Biest, S. Dillien. Texture and crystal orientation in Ti-6Al-4V builds fabricated by shaped metal deposition. Metall. Mater. Trans. A 2010, 41(8): 1917-1927.
[42] T. Vilaro, C. Colin, J.D. Bartout. As-fabricated and heat-treated microstructures of the Ti-6Al-4V alloy processed by selective laser melting. Metall. Mater. Trans. A 2011, 42(10): 3190-3199.
[43] L.E. Murr, S.M. Gaytan, E. Martinez, et al. Next generation orthopaedic implants by additive manufacturing using electron beam melting. Int. J. Biomater. 2012, 2012. https://doi.org/10.1155/2012/245727.
[44] ASM International. Handbook Committee. ASM handbook: Heat treating. Asm Intl. 1991.
[45] M.J. Blackburn, J.C. Williams. A comparison of phase transformations in three commercial titanium alloys (Phase transformations in commercial titanium alloys compared for mechanical properties, emphasizing decomposition of metastable beta phases on quenching, aging or deformation). ASM Trans. Q. 1967, 60: 373-383.
[46] P.J. Fopiano, M.B. Bever, B.L. Averbach. Phase transformations during the heat treatment of the Alloy Ti-6AI-4V. Trans. ASM 1969, 62: 324.
[47] R.Z. Valiev, I.V. Alexandrov, Y.T. Zhu, T.C. Lowe. Paradox of strength and ductility in metals processed by severe plastic deformation. J. Mater. Res. 2002, 17(01): 5-8.
[48] L. Liu, P. Kamm, F. García-Moreno, J. Banhart, D. Pasini, Elastic and failure response of imperfect three-dimensional metallic lattices: the role of geometric defects induced by Selective Laser Melting, J. Mech. Phys. Solids. 107 (2017) 160-184. https://doi.org/10.1016/j.jmps.2017.07.003.
[49] Z. Wang, J. Zhang, S.J. Li, W.T. Hou, Y.L. Hao, R. Yang, Effects of part size on microstructure and mechanical properties of Ti-6Al-4V alloy fabricated by Electron Beam Melting, Rare Metal Mat. Eng. 2014; 43:161-164. https://doi.org/1002-185X(2014)S1-161-04
[50] C. Ran, P.W. Chen, L. Li, W.F. Zhang, Y.L. Liu, X. Zhang, High-strain-rate plastic deformation and fracture behaviour of Ti-5Al-5Mo-5V-1Cr-1Fe titanium alloy at room temperature, Mech. Mater. 116 (2018) 3-10. https://doi.org/10.1016/j.mechmat.2017.08.007.
[51] W.-S. Lee, C.-F. Lin, Plastic deformation and fracture behaviour of Ti–6Al–4V alloy loaded with high strain rate under various temperatures, Mater. Sci. Eng. A. 241 (1998) 48-59. https://doi.org/10.1016/S0921-5093(97)00471-1.
[52] Z. Zhang, H. Sheng, Z. Wang, B. Gludovatz, Z. Zhang, E.P. George, Q. Yu, S.X. Mao, R.O. Ritchie, Dislocation mechanisms and 3D twin architectures generate exceptional strength-ductility-toughness combination in CrCoNi medium-entropy alloy, Nat. Commun. 8 (2017)

14390. https://doi.org/10.1038/ncomms14390.